Science of the Total Environment 829 (2022) 154636

Contents lists available at ScienceDirect

Science of the Total Environment

journal homepage: www.elsevier.com/locate/scitotenv

Temperature and precipitation dominates millennium changes of eukaryotic algal communities in Lake Yamzhog Yumco, Southern Tibetan Plateau

Shouliang Huo [a,b,*], Hanxiao Zhang [a,b], Jingfu Wang [c], Jingan Chen [c], Fengchang Wu [b]

[a] State Key Laboratory of Environmental Criteria and Risk Assessment, Chinese Research Academy of Environmental Sciences, Beijing 100012, China
[b] College of Water Sciences, Beijing Normal University, Beijing 100012, China
[c] State Key Laboratory of Environmental Geochemistry, Institute of Geochemistry, Chinese Academy of Sciences, Guiyang 550081, China

HIGHLIGHTS

- Millennium changes of eukaryotic algal community have been revealed.
- SEM was are used to quantify how climate change drives algae productivity and community.
- Temperature and precipitation dominates the succession of eukaryotic algal community.
- These findings provide important basis for lake protection strategy of Tibet Plateau.

GRAPHICAL ABSTRACT

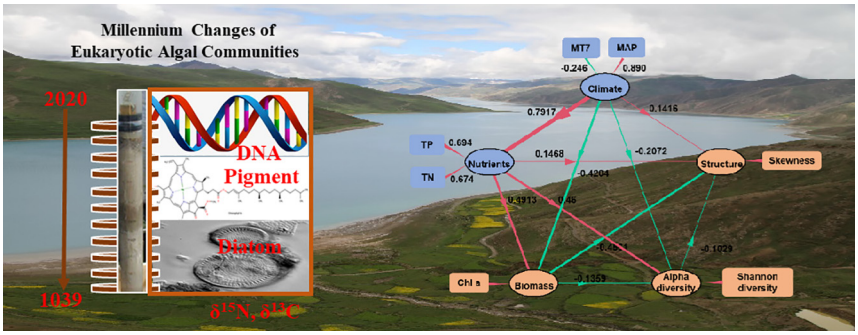

ARTICLE INFO

Article history:
Received 9 January 2022
Received in revised form 22 February 2022
Accepted 13 March 2022
Available online 17 March 2022

Editor: Ouyang Wei

Keywords:
Climate change
Tibetan Plateau
Eukaryotic algae
Nutrient loading

ABSTRACT

Despite significant climate change on the Tibetan Plateau, the historical succession trend and underlying driving mechanism of aquatic ecosystem in alpine lake remain unclear. In this study, palaeolimnological analysis and high-throughput sequencing of sedimentary DNA were used to investigate environmental changes, primary productivity, and eukaryotic algal community succession over the past millennium in Lake Yamzhog Yumco of the southern Tibetan Plateau. Lake primary productivity significantly increased after ~1850 CE and algal community succession occurred in three stages including the Medieval Warm Periods (approximately 1000–1250 CE), the Little Ice Age (1250–1850 CE), and the Current Warm Period (1850–2020 CE). Moreover, succession was synchronous with inferred climate changes. Partial least square path modeling indicated that climate factors affected primary productivity and eukaryotic algal community structure by affecting nutrient loading. The results suggest that glacier melting and permafrost degradation caused by climate warming, combined with increased precipitation, may be the major driving factors of nutrient concentration increases, phytoplankton biomass increases, and shifts in community composition. Considering the expected trends of future climate change and continuous warming, the restoration of vegetation cover and reduction of non-point source nutrient loading in the Tibetan Plateau is urgently needed to mitigate climate change impacts on alpine lake aquatic ecosystems.

1. Introduction

The Tibetan Plateau is referred to as the "the World's Third Pole" and exhibits an average elevation of over 4000 m asl. The plateau is also known as "the Asian water tower" due to harboring 36,800 glaciers and 1171 lakes that are >1 km^2 in area. The area comprises the headstream region of many major rivers, including the Yangtze, Yellow, Lancang, Brahmaputra,

* Corresponding author at: State Key Laboratory of Environmental Criteria and Risk Assessment, Chinese Research Academy of Environmental Sciences, Beijing 100012, China.
E-mail address: huoshouliang@126.com (S. Huo).

http://dx.doi.org/10.1016/j.scitotenv.2022.154636

Ganges, and Indus rivers, which nourish hundreds of millions of people throughout Asia (Royden et al., 2008; Yao et al., 2012; Tao et al., 2020). The Tibetan Plateau has undergone significant climate change since the Anthropocene, a human-dominated geological epoch beginning around 1610 (Lewis and Maslin, 2015), including a 0.2 °C temperature increase per decade over the past 50 years, representing a rate of increase about twice that observed for global warming, which has considerably accelerated glacier melt and permafrost degradation (Yang et al., 2010; Pepin et al., 2015; Wu et al., 2015; Zou et al., 2017). The evident warming on the Tibetan Plateau over the past few decades has led to the expansion of most lakes that are primarily fed by glacier melt, while a few lakes on the southern Tibetan Plateau that are primarily supplied by precipitation have exhibited decreased lake areas due to intensified evaporation (Zhang et al., 2011, 2017, 2020; Nie et al., 2017; Qiao et al., 2019). Lakes are crucial sensors and regulators of climate change that can influence hydrological cycles in addition to regional biotic and abiotic environments on the Tibetan Plateau via complex cryospheric-hydrological-geodynamic processes (Qiao et al., 2019; Woolway et al., 2020; Liang et al., 2021). Substantial efforts have been made towards understanding water storage and cycling in Tibetan Plateau lakes using Landsat data in addition to laser or radar altimetry (Yang et al., 2014; Zhang et al., 2011, 2017, 2020; Nie et al., 2017; Qiao et al., 2019). Nevertheless, few studies have traced aquatic ecological succession and their responses to climate change in remote and inaccessible mountain regions.

Phytoplankton are key contributors to biogeochemical cycles in addition to energy and matter cycling through food chains since they are the major aquatic primary producers and are the most sensitive indicators of lake environmental change (Strom, 2008; Righetti et al., 2019). Previous limnological studies have focused on patterns of phytoplankton succession and their responses to environmental change in mesotrophic lakes that are affected by human activities (Posch et al., 2012; O'Beirne et al., 2017; Monchamp et al., 2018; Wang et al., 2019; Ibrahim et al., 2020; Zhang et al., 2021a, 2021b). Phytoplankton dynamics are primarily regulated by bottom-up, such as nutrient levels, light and temperature (Righetti et al., 2019; Zhang et al., 2021a). However, knowledge gaps remain regarding patterns of phytoplankton community assembly in alpine lakes that are characterized by large diurnal and seasonal variation in air temperature, in addition to obvious contrasts of water-heat balance in cold and warm seasons (Tao et al., 2020). Moreover, Tibetan Plateau lakes are sensitive to climate change, while also featuring less disturbance by human activities, providing an important model to study the responses of phytoplankton succession on climate-induced environmental changes (Chen et al., 2013).

A significant challenge in understanding alpine lake ecosystems is that little information is available on time- scales sufficient to assess long-term, centennial- to millennial-level changes in water quality and the biotic communities of aquatic ecosystems (Monchamp et al., 2018; Ibrahim et al., 2020). Lake sediments, as natural 'storage rooms or boxes' for entire basins, can be used to reconstruct information for long-term dynamics of aquatic ecosystems via analysis of multiple physicochemical proxies, fossils, and pigments (Tse et al., 2018). Lake sedimentary DNA (*sed*DNA) analysis has recently emerged as an alternative strategy to reconstruct past biotic succession via highly accurate and comprehensive species identification, as diagenetic processes occurring during burial in sediments have limited effects on DNA degradation (Anderson-Carpenter et al., 2011; Capo et al., 2017; Domaizon et al., 2017; Monchamp et al., 2018; Keck et al., 2020). Strict and normalized protocols for *sed*DNA extraction and amplification have been developed to overcome problems arising from DNA degradation, low DNA yields, and modern DNA contamination. Indeed, these methods have been successfully used to reconstruct the succession of numerous prokaryotic and eukaryotic aquatic organisms, including Cyanobacteria (Monchamp et al., 2018; Zhang et al., 2021a, 2021b), diatoms (Ibrahim et al., 2020), zooplankton, and many other micro-eukaryotic groups (Capo et al., 2017; Domaizon et al., 2017; Keck et al., 2020).

In the present study, coupled paleolimnological approaches and high-throughput sequencing of *sed*DNA were applied to evaluate the succession of aquatic environments and composition of eukaryotic algal communities over the past 2000 years in Lake Yamzhog Yumco in order to understand algal community succession in alpine lakes of the Tibetan Plateau. We hypothesized that climate change was the major driving factor underlying succession of eukaryotic algal communities since lakes on the Tibetan Plateau are less disturbed by human activity (Tao et al., 2020). The primary objectives of this study were to (i) identify temporal trends of nutrient states and primary productivity in Lake Yamzhog Yumco; (ii) reconstruct the temporal succession of eukaryotic algal communities of the lake and identify temporal changes in their composition, diversity, structure, and ecological networks across the past millennium; and (iii) explore the effects of long-term climate change and nutrient states on eukaryotic algal communities.

2. Materials and methods

2.1. Study site

Lake Yamzhog Yumco (28°27′–29°12′N, 90°08′–91°45′E, average altitude of 4440 m) is a holy lake in Tibet and is located in the southern Tibetan Plateau in the northern foothills of Himalayas with a lake surface area of 599.9 km^2 and a maximum water depth of 59 m (Guo et al., 2018). The region is characterized by a currently semi-arid climate with a mean annual temperature of 2.9 °C (minimum average temperature in January of −4.8 °C and maximum in July of 10.1 °C), in addition to a mean annual precipitation of 370 mm (Sun et al., 2021). About 90% of annual precipitation occurs in summer (June to September). The basin is primarily covered with alpine steppe and alpine meadow ecosystems that occur over elevations of between 4500 and 4900 m and 4900–5200 m, respectively (Zhe and Zhang, 2021). Lake Yamzhog Yumco waters are mainly supplied by precipitation and the lake has shrunk by 11.39% since 1974, as warming temperatures and intensified evaporation have concomitantly occurred (Zhe et al., 2017). Hydrochemical data from 2009 to 2014 indicate that lake waters are weakly alkaline (pH 8.38–9.49 with total hardness values >500 mg L), and brackish (total dissolved solids 1065.71 mg L) (Zhe et al., 2017). The Yamzhog Yumco Pump Storage Power Station is located on the north shore of the lake and began operation in 1998 to produce electricity when lake water spills down to the Yarlung Zangbo River and also to pump water from the Yarlung Zangbo River back to Yamzhog Yumco in order to maintain water levels (Sun et al., 2021). The basin comprises the largest lake region in the middle reaches of the Yarllung Zangbo valley in the Black-necked Crane National Nature Reserve and provides critical water resources for local people and wildlife. Under the human activities and climate warming, if the algal community changes to the harmful algae dominant community, it will have a profound impact on ecosystem functioning and services (Righetti et al., 2019). It is consequently urgent to understand the successional history of the lake aquatic environment and its algal communities over time.

2.2. Sediment coring, dating, and multiproxy analysis

Sediment core were collected from the center of the lake (Fig. S1; 28°56′15.36″N, 90°40′27.48″) using a gravity corer (inner tube diameter of 5.9 cm, length of 120 cm) on July 2020, while the upper 40 cm of sediment was sectioned into 40 slices of 1 cm thickness. Core chronology was obtained through a combination of ^{210}Pb and ^{137}Cs dating on the upper 10 cm of sediment in addition to two AMS^{14}C dates from plant residues at the 32 cm and 40 cm layers in the core (Guo et al., 2018). The two AMS^{14}C dates were calibrated to calendar years using the CALIB 6.0 program IntCal 13 dataset (Reimer et al., 2013), and the age-depth model of Lake Yamzhog Yumco was established according to a 2nd-order polynomial regression model (Fig. S2). Total phosphorus (TP) in the core sections was extracted by adding 3.5 M HCl in 0.2 g freeze-dried sample in a porcelain crucible after ashing at 500 °C for 2 h, followed by measurement with the ascorbic acid method (Murphy and Riley, 1962). Total organic carbon (TOC) and total nitrogen (TN) were determined using a Vario MACRO elemental analyzer (Elementar Corporation, Hanau, Germany), after inorganic carbonate was removed by 1 M HCl prior to TOC determination (Solorzano

and Sharp, 1980). $\delta^{13}C_{org}$ was measured with a gas isotope ratio mass spectrometer (MAT 253, Thermo Fisher, USA, accuracy <0.1‰) after acidification with 1 M HCl (Carter and Fry, 2013). Results are expressed in standard per mill units, relative to international standards Vienna PeeDee Belemnite (Carter and Fry, 2013).

About 1 g of homogenized freeze-dried sediment was used to extract pigments from 3 mL of acetone-water mixtures (95:5 v:v). The solutions were ultrasonicated in an ice water bath for 15 min and then left in the dark for 24 h. Extractions were filtered using a 0.22 μm PTFE filter and characterized using an Agilent 1200 series high performance liquid chromatograph (HPLC) instrument equipped with an auto-sampler (Model G1315C) and a diode-array detector (Agilent Technologies Inc., Palo Alto, CA, USA) (Jiang et al., 2017). Nineteen pigment standards were obtained from DHI Inc. (Hørsholm, Denmark) and used as references, including the chlorophylls Chlorophyll *a* (Chl *a*), Chlorophyll *b* (Chl *b*), Mg-2,4-divinylpheoporphyrin (MgDVP), pheophytin *a*, and pheoporbide *a*; the carotene *β*,*β*-carotene; and xanthophylls including Alloxanthin, 19-Butanoyloxyfucoxanthin (But-fuco), Canthaxanthin, Diadinoxanthin, Diatoxanthin, Fucoxanthin, 19-Hexanoyloxyfucoxanthin (Hex-fuco), Lutein, Neoxanthin, Peridinin, Prasinoxanthin, Violaxanthin, and Zeaxanthin. Additional details of pigment analyses have been previously described (Zhang et al., 2019). All pigment concentrations are expressed as micrograms per gram of dry sediment (μg g^{-1} dry sediment).

A two-component multi-G model was used to estimate pigment degradation in Lake Yamzhog Yumco. The model divides organic matter into several components, each with a unique rate of degradation (Li et al., 2015). Specifically, Phaeophytin *a* and Phaeophorbide *a* are degradation products of Chl *a* and belong to the chlorins class of molecules (Liang et al., 2021). The multi-G model equation is as follows:

$$C_t = C_\infty + C_0 \times (1-a) \times e^{(-k_1 \times t)} + C_0 \times a \times e^{(-k_2 \times t)} \quad (1)$$

where C_0 (167.0 μmol/g OC) and C_∞ (19.6 μmol/g OC) are organic matter contents in surface sediments and at infinite depths, respectively, while C_t represents organic matter contents at time t (years). k_1 and k_2 are the degradation rates of the two degradation products and were set as 0.002 and 0.3, respectively (Li et al., 2015). a represents the refractory portion in the organic matter ($a = 0.7$) and t can be calculated by dividing layer depth d (cm) by sedimentation rate, s (0.041 cm yr^{-1}).

2.3. Molecular analyses

Strict laboratory procedures for DNA extraction and PCR amplification were followed to ensure the validity of sequencing data. Specifically, experimental operating environments and instruments were sterilized to avoid sample contamination by modern DNA or cross-contamination. About 0.5 g of homogenized sediment for each sample was subjected to DNA extraction using a PowerSoil DNA Isolation Kit (MoBio, Carlsbad, USA). One blank control was conducted every six samples during DNA extraction, and all blank controls were negative, thereby confirming a low possibility of contamination from external DNA during extraction procedures. DNA extractions were quantified using a NanoDrop ND-2000 spectrophotometer (NanoDrop Technologies, Wilmington, DE, USA). Universal micro-eukaryote primers (960F: 5′-GGCTTAATTTGACTCAACRCG-3′; NSR1438: 5′-GGGCATCACA GACCTGTTAT-3′) were used to amplify ~260 bp fragments of the V7 hypervariable regions of 18S rRNA genes using a two-step PCR amplification procedure (Capo et al., 2017; Ibrahim et al., 2020; Zhang et al., 2021b). Paired-end sequencing data were first merged by FLASH v.1.2.7 (Magoč and Salzberg, 2011), and then filtered and clustered with several steps as described in our previous literature (Zhang et al., 2021a). The taxonomic affiliation of operational taxonomic units (OTUs) was performed using the RDP classifier within QIIME (Caporaso et al., 2010), based on the Silva databases (Pruesse et al., 2007). For comparison among samples, the OTU table was random rarefied to account for differences in sequencing depth using MOTHUR v.1.39.5 (Schloss et al., 2009). Alpha diversity values (i.e., OTU richness, Shannon / Simpson diversity indices, and Pielou evenness) of eukaryotic algal communities were estimated based on rarefied OTU tables using the 'vegan' package for R (Oksanen et al., 2020). Posterior probabilities to assess the presence of inflection points for alpha diversity indices over time were estimated using Bayesian change point (*bcp*) analysis in the 'bcp' package for R (Wang et al., 2018).

2.4. Statistical analyses

Historical trends for pigments and eukaryotic algal groups were visualized using Tilia (v2.2.1) and clustered using constrained incremental sums of squares cluster analysis (CONISS; Bennett, 1996). The timing and hierarchy of significant changes in eukaryotic algal community structures were further evaluated using multivariate regression tree (MRT) analysis with the 'mvpart' package for R (De'ath, 2002, 2014). The combination of the two clustering methods (CONISS and MRT) were used to identify change points in eukaryotic algal community structures at the taxonomic and OTU levels, respectively. The historical phases of eukaryotic algal community succession identified by the two clustering methods were temporally close to the basin climate periods comprising the Medieval Warm Period (MWP, approximately 800 to 1300 CE), the Little Ice Age (LIA, approximately 1300–1850 CE), and the Current Warm Period (CWP, approximately 1850 CE to the present) identified in previous studies (Guo et al., 2018). To verify changes among eukaryotic algal community structures across different historical periods, analysis of similarities (ANOSIM) and permutational multivariate analysis of variance (PERMANOVA) was used to investigate differences in community composition across phases (based on Jaccard dissimilarities) using 999 Monte Carlo permutations (Ramette, 2007; Anderson, 2014). Ordinations of eukaryotic algal community structures were evaluated using distance-based redundancy analysis (dbRDA) of principal coordinates analysis (PCoA) based on Bray-Curtis dissimilarities among communities using the *rda* function of the'vegan' package. Mean annual precipitation (MAP), July temperature (MT7), and relative humidity (HHH) were climate variables established by pollen-based quantitative reconstructions (Guo et al., 2018), and were corresponding to the chronology of this study through interpolation processing (Fritsch and Carlson, 1980).

Network analysis was used to identify cooccurrence patterns among OTUs in communities. Two co-occurrence networks were constructed based on Spearman's correlations and Cramér's association degree of OTU relative abundances across samples. Spearman's correlations between two OTUs were considered statistically robust if correlation coefficients $r > 0.5$ and $p < 0.01$ (Berry and Widder, 2014). A false discovery rate (FDR) correction was applied to adjust *p*-values to control for false-positive results. Co-occurrence networks were constructed using the Fruchterman-Reingold algorithm and visualized using the Gephi software program (v.0.9.2). Network metrics were calculated to estimate network topological properties, including average degree, average path length, clustering coefficients, density, diameter, and weighted modularity. Moreover, the OTU pairs in the top 50% of the Cramér's correlation degree distribution were considered connected pairings and used to construct another network (Wang et al., 2019). The skewness in OTU degree and clustering coefficients were calculated to evaluate asymmetry in the frequency distribution of OTU co-occurrences and the realized fraction of all possible co-occurrences between OTUs linked to a common network, respectively.

The relationships between climate variables, nutrient concentrations, algal biomass, alpha diversity, and eukaryotic community structures were further explored using partial least squares path modeling (PLS-PM) with the 'plspm' package for R (Wang et al., 2016). The model represents the partial least squares approach to structural equation modeling (SEM) and is an appropriate statistical framework to test hypotheses about complex cause-effect relationships among multiple drivers and response variables. Pairwise evaluation of variables with correlational analysis and regression analysis was used to exclude insignificant and highly collinear variables.

Five groups of variables were ultimately selected and used for modeling including climate variables (mean annual precipitation and July temperature), nutrient concentrations (sedimentary total nitrogen and total phosphorus), algal biomass (indicated by sedimentary Chl *a*), alpha diversity (the Shannon diversity index), and the structure of eukaryotic algal communities (modeled by skewness of OTU degree in co-occurrence networks). PLS-PM models were conducted using 999 bootstraps to verify the direct and indirect influences of predictor variables on eukaryotic algal communities. The direction and strength of the linear relationships between variables were indicated by path coefficients. Indirect effects are represented by the multiplied path coefficients between a predictor and a response variable when adding the product of all possible paths excluding the direct effect (Wang et al., 2016). The performance of the model was evaluated using the goodness-of-fit (GOF) index.

3. Results

3.1. Temporal trends in climate and trophic states

The Lake Yamzhog Yumco core could be divided into three major units according to stratigraphic observations including: a gray-white silt layer (40–34 cm), a gray-brown clay-silt layer (34–13 cm), and a gray-white silt-sand layer (13–0 cm). The chronology of the core was constructed by ^{137}Cs and ^{210}Pb analysis, and calibrated by AMS^{14}C dating (Guo et al., 2018). Excess ^{210}Pb ($^{210}Pb_{ex}$) activities from the top 10 cm exhibited an approximately exponential decrease with minor fluctuations, which may be related to lithological changes (Fig. S2). The constant rate of supply (CRS) model based on exponential simulation of $^{210}Pb_{ex}$ activities and mass depth indicated that the average sedimentation rate and the average mass sedimentation rate were 0.0448 cm yr^{-1}and 0.00278 g cm^{-2} yr^{-1}, respectively. The ^{137}Cs range of the core is 0–12.5 Bq kg^{-1} (Fig. S2). ^{137}Cs peaked at 3 cm (corresponding to 0.16 g cm^{-2} mass depth) and then gradually decreased to nearly zero, which is an ideal deposition curve. Assuming that the corresponding year of the main accumulation peak is 1963, the average sedimentation rate is 0.0439 cm yr^{-1}, and the average mass sedimentation is 0.00281 g cm^{-2} yr^{-1}, consistent with the $^{210}Pb_{ex}$-based estimations. The dating data from ^{137}Cs and $^{210}Pb_{ex}$ estimations span a total of 286 years at 1–10 cm, ranging from 1734 to 2020 CE, similar to estimations from a previous study using AMS^{14}C dating (Guo et al., 2018) that was used to construct an age-depth model with a 2nd-order polynomial regression model, leading to an estimated age of the bottom sample being extrapolated as approximately 1039 CE (Fig. S2).

The MAP, MT7, and HHH parameters estimated from the Yamzhog Yumco Lake core were reconstructed from 23 major pollen taxa in the Tibetan Plateau and indicated that the climate in the area was warm and dry during the MWP (780–1300 CE) and the CWP (1850 CE–present), but cold and moist during the LIA (1300–1850 CE) (Fig. 1a; Guo et al., 2018). The average MT7, MAP, and HHH values during the MWP were 15 °C, 455 mm, and 52%, respectively, but 14 °C, 540 mm, and 56% during the LIA, respectively. MT7 increased after ~1850 CE, while MAP and HHH decreased. The climate in Yamzhog Yumco basin can thus be characterized by warm-dry and cold-moist patterns across the past two millennium that are influenced by mid-latitude westerlies, the Indian summer monsoon, and the East Asian summer monsoon (Guo et al., 2018).

Geochemical proxies, including TOC, TN, TP, $\delta^{13}C_{org}$, and C_{org}: N, were used to estimate long-term trends in the trophic states and sources of organic matter (OM) in core samples (Fig. 1a). TOC, TN, and TP contents were relatively high during the MWP and then significantly increased during the CWP. The average $\delta^{13}C_{org}$ values during the MWP, LIA, and CWP periods were − 22.55‰, −23.73‰, and − 26.53‰, representing a decreasing trend likely associated with increased photosynthesis. Mean values of C_{org}:N ratios during the MWP, LIA, and CWP periods were 6.72 ± 0.25 (mean ± standard deviation), 6.31 ± 0.77, and 5.85 ± 0.24, respectively, suggesting that sediments were dominated by algal-sourced OM (as indicated by C_{org}:N < 10). A cross-plot of C_{org}: N and $\delta^{13}C_{org}$ also suggested that autochthonous primary productivity was the dominant influence on the sedimentary organic record of the lake (Fig. 1b).

3.2. Temporal changes in historical primary productivity

The absolute concentrations of fossil pigments provide a credible record of lacustrine primary productivity when the sediments are well-preserved (Jiang et al., 2017; Zhang et al., 2019). Good pigment preservation was indicated by a low ratio of pheopigment *a* (the sum of pheophytin *a* and pheoporbide *a* that are degradation products of Chl *a*) to Chl *a,* which ranged from 0 to 0.353 in the Lake Yamzhog Yumco core (Fig. 2b). The ratio of total carotenoids to total identified pigments in the 0–6 cm sediment layer (0.429 ± 0.057, mean ± SD) was higher than that in the 7–40 cm sediment layer (0.343 ± 0.028), indicating that pigment preservation was better in the upper layer than in the bottom layer. However, Multi-G modeling of pigment degradation demonstrated that the relative abundances of pigments were not strongly affected by degradation, although slight degradation of pigments was observed in sediments below 6 cm (Fig. 2c). These results can generally be interpreted to support the conclusion that pigment preservation accurately reflected historical primary productivity in the lake over the period studied here.

Nineteen pigments were detected in the Lake Yamzhog Yumco core sediments (Fig. 2a). Pigment contents (excluding the degradation products of Chl *a*: MgDVP, pheophytin *a*, and pheoporbide *a*) varied little before the mid-1800s, but substantially increased afterwards. Indeed, a significant difference was observed in the sedimentary pigments before and after ~1850 CE according to CONISS analysis (Fig. 2a) that could be attributed to increased primary productivity. Chl *a* content increased from 26.83 ± 8.17 (mean ± SD) μg pigment g^{-1} sediment in the first stage to 105.03 ± 36.80 μg pigment g^{-1} sediment in the second stage. Individual pigments associated with different taxa have often been used to track temporal distributions of specific algal community members (Table S1). The most abundant specific pigments were Fucoxanthin (primarily derived from diatoms), Peridinin (from dinoflagellates), Zeaxanthin (from Cyanobacteria), and Chl *b* (from green algae), which exhibited profile means of 10.70, 7.26, 3.49, and 3.23 μg pigment g^{-1} sediment, respectively. Thus, the potentially dominant algae of the system included diatoms, dinoflagellates, Cyanobacteria, and green algae (Roy et al., 2011; Zhang et al., 2019).

3.3. Historical succession of eukaryotic algal communities

High-throughput sequencing of environmental DNA from lake sediments provides a taxonomically sensitive method to reconstruct historical eukaryotic algal compositions of lakes. A total of 453,939 18S rRNA gene sequences were obtained from 40 samples of the Lake Yamzhog Yumco core after quality filtering and these comprised 372 eukaryotic OTUs. OTUs classified as non-eukaryotic algae were discarded to specifically focus on eukaryotic algal populations that ultimately comprised 52,347 reads that clustered into 79 OTUs (Table 1). Evidence of DNA degradation was not observed among taxa based on the number of OTUs and sequences that were recovered (Fig. 3). Combined with results from previous studies that used sedimentary DNA to investigate long-term dynamics of lake biodiversity, DNA decay may be of marginal concern at the millennium time scale, while differences in DNA cross-layer preservation is unlikely to also be significant on this scale (Capo et al., 2017; Keck et al., 2020; Zhang et al., 2021a and 2021b).

Most sequences were classified as Bacillariophyceae, Fragilariophyceae, Mediophyceae, Chlorophyceae, Trebouxiophyceae, Chrysophyceae, Cryptophyta, Dinophyceae, Eustigmatophyceae, Phaeophyceae, and Rhodophyta (Fig. 3). Chlorophyceae was the most dominant eukaryotic algal group, with average relative abundances of 22.43%, followed by Mediophyceae (13.78%), Dinophyceae (12.36%), and Cryptophyta (11.14%). Significant changes in eukaryotic algal community composition were detected at ~1850 CE and ~ 1250 CE based on CONISS analysis (Fig. 3). Specifically, simultaneous increases in the relative abundances of Bacillariophyceae and Trebouxiophyceae were observed after ~1850 CE,

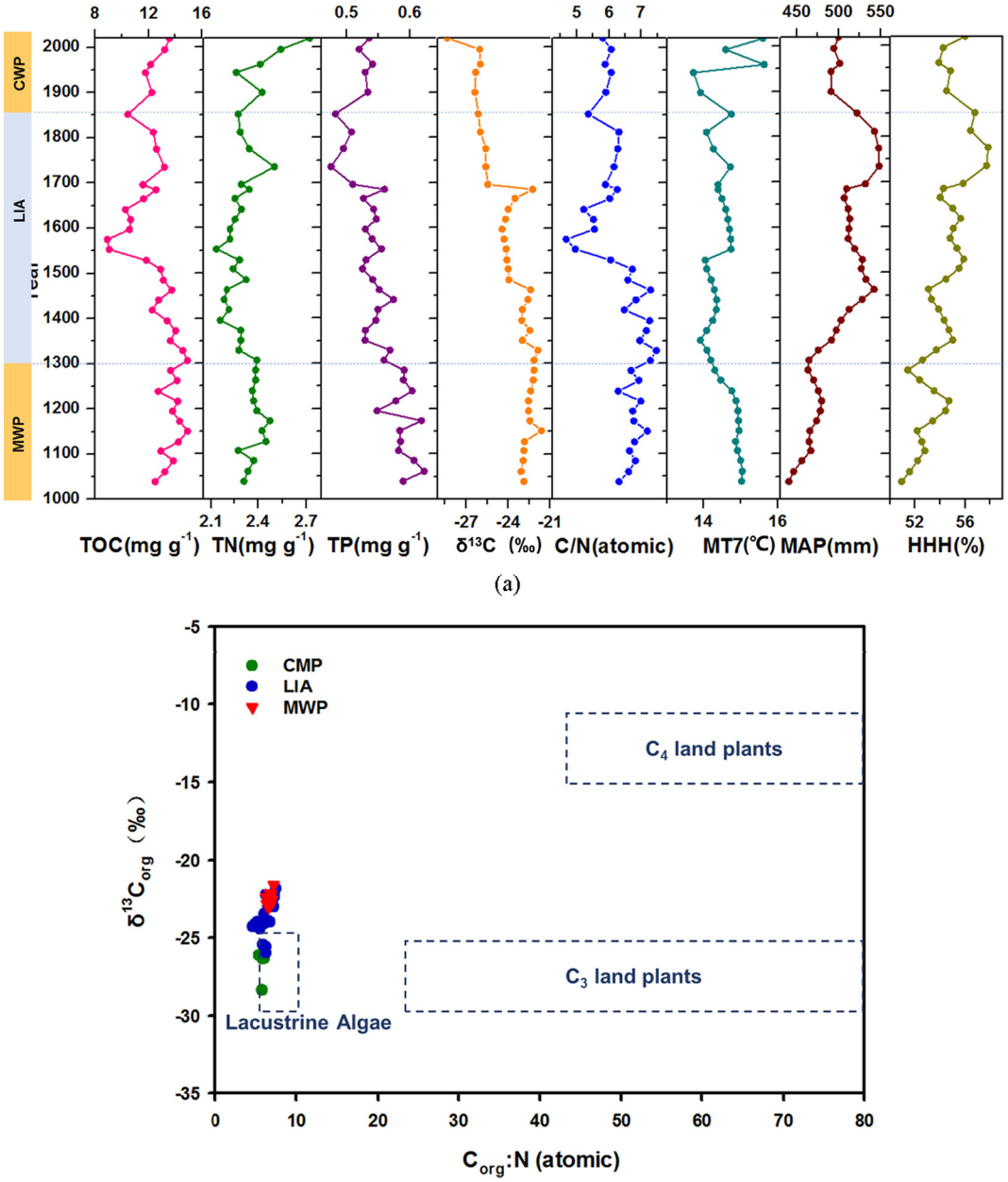

Fig. 1. (a) Temporal trends in the concentration of paleovariables, including sedimentary TOC, TN, TP, δ13Corg, C/N(atomic), and climate variables established by pollen-based quantitative reconstructions, including the July temperature (MT7), mean annual precipitation (MAP), and relative humidity (HHH). (b) Cross-plot of 13Corg: N versus δ13Corg showing values plot within the lacustrine algal range of the three historical periods. MWP, LIA, and CWP represent the Medieval Warm Period, Little Ice Age, and Current Warm period, respectively. Refer to Guo et al. (2018) for data of climate variable.

concomitant with a gradual decrease in Fragilariophyceae, Mediophyceae, and Chlorophyceae relative abundances. Consequently, three successional stages of eukaryotic algal communities were estimated at approximately 1000–1250 CE, 1250–1850 CE, and 1850–2020 CE, consistent with variation in climate indices and sedimentary geochemical proxies (Fig. 1, Fig. 2, Fig. 3).

Eukaryotic algal community alpha diversity did not systematically decrease across time, as indicated by OTU richness in addition to the Shannon and Simpson diversity indices, along with the Pielou evenness index (Fig. 4A). Nevertheless, estimated OTU richness varied over time, ranging from 16 to 65, with significant increases following ~1685 CE. An inflection point for the Pielou evenness index was observed at ~1553 CE, followed by significant decreases afterwards. Inflection points were not detected for the Shannon and Simpson diversity indices over time, indicating relatively stable diversity trends across the past millennium (Fig. 4A). MRT analysis demonstrated that eukaryotic algal community structures significantly differed before and after 1850 CE, consistent with CONISS analysis (Fig. 4B). Beta diversity analysis further indicated a significant change in community structure among the CWP, LIA, and MWP stages based on ANOSIM and PERMANOVA analysis of Jaccard metric community differences (ANOSIM $R = 0.198$, $P = 0.001$; PERMANOVA pseudo-$F = 2.05$, $P = 0.003$). Variation in community structure was also further characterized by network analysis, since biodiversity is an incomplete indicator of exogenous forcing, such as nutrient loading and climate warming (Wang et al., 2019). Under the human impact and climate change, environmental homogenization leads to higher species connectivity in similar microhabitats, presenting a co-occurrence network with negative skew of species degree and high clustering coefficient (Wang et al., 2019). The frequency distribution of nodal degree gradually changed from positive skewness under an unstressed environment to negative skewness in a stressed environment with time (Fig. 5).

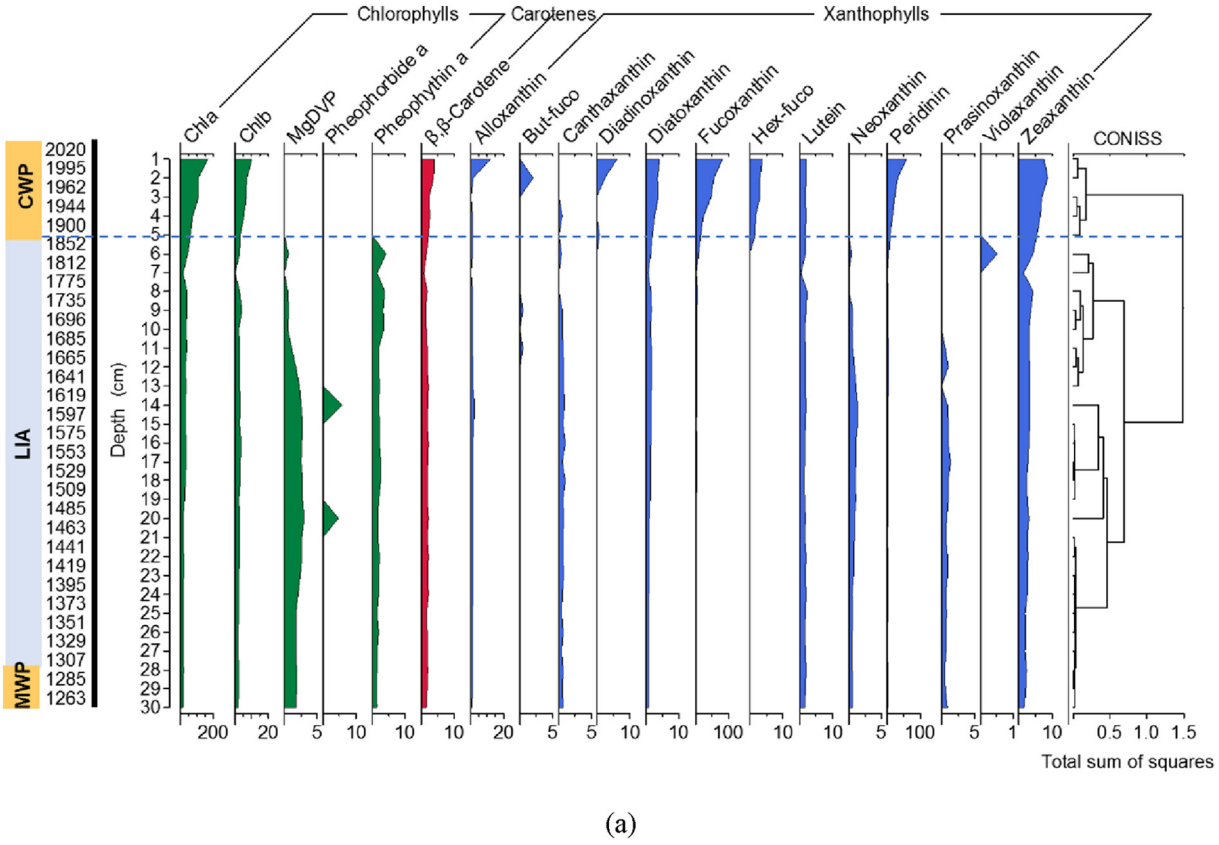

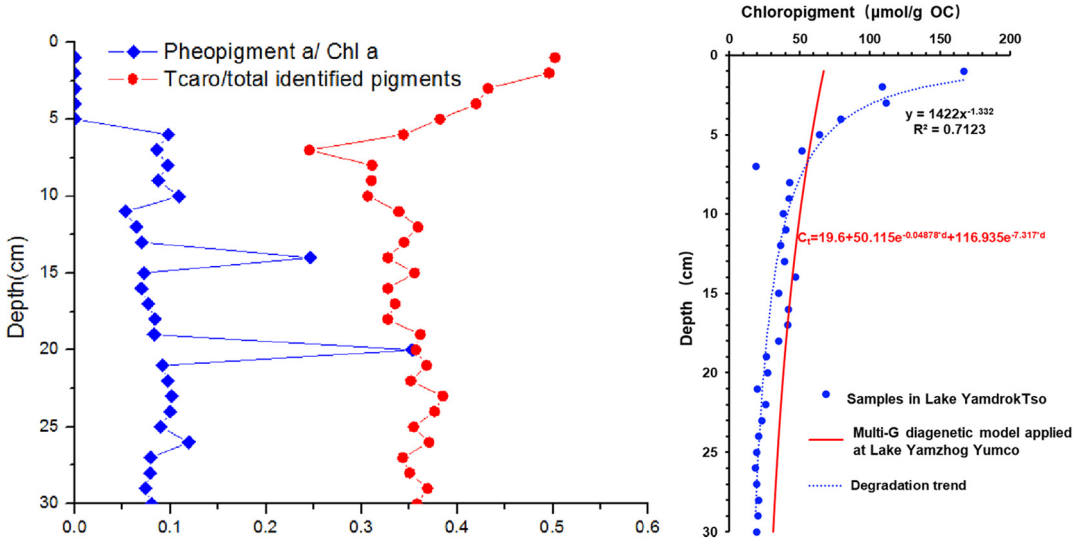

Fig. 2. Profiles of phytoplankton pigments (a), pigment degradation indicators (b), and the comparison of chloropigment concentrations with pigment degradation trends simulated by Multi-G model (c) from core sample in Lake Yamzhog Yumco (c). All compounds are expressed as ug pigment g^{-1} sediment. The right panel shows results from constrained incremental sums of squares cluster analysis (CONISS) based on the contents of pigments among different layers. MWP, LIA, and CWP represent the Medieval Warm Period, Little Ice Age, and Current Warm period, respectively.

More specifically, the skewness values of OTU associations ranged from −0.523 to 0.948 and generally decreased over time, while the clustering coefficients ranged from 0.138 to 0.448 and increased over time, especially during the CWP (Fig. 5).

3.4. Key drivers involved in historical state changes

The historical succession of eukaryotic algal communities may be driven by nutrient loading and climate change. *sed*DNA-based community changes were consequently compared against geochemical proxies for lacustrine environmental dynamics, pigments as proxies for primary productivity, and climate variables as representatives of climatic forcing. These analyses were used to evaluate the correlation between lacustrine environmental patterns and eukaryotic algal community responses to variation in nutrient loading and climate change during the three observed successional stages (Fig. S3). Climate variables (MT7, MAP, and HHH), and nutrient proxies (sedimentary TN, TP, and TOC) exhibited different degrees of correlation with primary productivity, community diversity, and eukaryotic

Table 1
The table presents for the number of DNA sequences, OTUs within each eukaryotic algae group, and the percentage within each taxonomic group.

Taxonomic groups		DNA sequences	OTUs	Percentage (%)
Bacillariophyta	Bacillariophyceae	3692	9	7.05
	Fragilariophyceae	914	3	1.75
	Mediophyceae	7213	7	13.78
	Other Bacillariophyta	36	2	0.07
Chlorophyta	Chlorophyceae	11,740	19	22.43
	Trebouxiophyceae	5057	7	9.66
	Other Chlorophyta	2637	4	5.04
Chrysophyceae		4242	11	8.1
Cryptophyta		5830	2	11.14
Dinophyceae		6471	11	12.36
Eustigmatophyceae		1239	1	2.37
Phaeophyceae		1568	1	3
Rhodophyta		1708	2	3.26

algal community structures, wherein the correlations across the three successional stages gradually became stronger over time (Fig. S3). Correlations between eukaryotic algal communities and environmental variables were further assessed by dbRDA ordination analysis. The environmental variables explained 64.68% of the variation in eukaryotic algal community structures. The MAP, HHH, MAT, TN, and TP parameters exhibited significant correlations with eukaryotic algal distributions, as indicated by smaller angles between environmental vectors and the ordination axis (Fig. S4).

Co-occurrence patterns of eukaryotic algal taxa and environmental characteristics were analyzed by correlation-based network analysis to assess their associations (Tse et al., 2018). The network consisted of 86 nodes connected by 324 edges, with an average node degree of 7.535 (Fig. S5). The OTUs with the highest degrees in the network were OTU7 (Dinophyceae), OTU27 (Bacillariophyceae), OTU29 (Bacillariophyceae), OTU70 (Trebouxiophyceae), OTU73 (Trebouxiophyceae), and OTU75 (Trebouxiophyceae). The clustering coefficients of the network were 0.748, indicating the presence of modular structures (i.e., > 0.4) (Newman, 2006). Three major modules comprised 26.74%, 16.28%, and 9.3% of the nodes, respectively. Overall, the networks comprised highly connected nodes that were structured among densely connected modules that formed clustered topologies. Associations or interactions between specific eukaryotic algal taxa and a variety of environmental variables including TP associated with OTU7 (Dinophyceae), OTU30 (Bacillariophyceae), and OTU32 (Bacillariophyceae). Although such associations may not be clearly interpreted for co-occurrence versus causation of a given variable, these structures nevertheless provide insights that can be used to retrospectively assess relationships between taxa and environmental characteristics (Newman, 2006; Tse et al., 2018).

Linkages between eukaryotic algal community succession and significantly associated contextual environmental variables were further synthetically illustrated by PLS-PM models in the three successional stages across the entire period. It should be noted that the limitation of different sample size on the performance of the four PLS-PM models (Hair et al., 2019). During the MWP stage, the effects of each path were not very strong, with absolute path coefficient values between 0.10 and 0.38 (Fig. 6a). In the LIA stage, climate variables exhibited positive effects on nutrient levels and primary productivity, with path coefficients of 0.436 and 0.633, respectively (Fig. 6b). During the CWP stage, nutrient levels affected primary productivity and eukaryotic algal community structures, while primary productivity also exhibited strong effects on eukaryotic algal communities (Fig. 6c). Across the entire study period, climate variables were the dominant factors directly or indirectly affecting nutrients, primary productivity, and eukaryotic algal communities (Fig. 6d). These results document the direct effects of

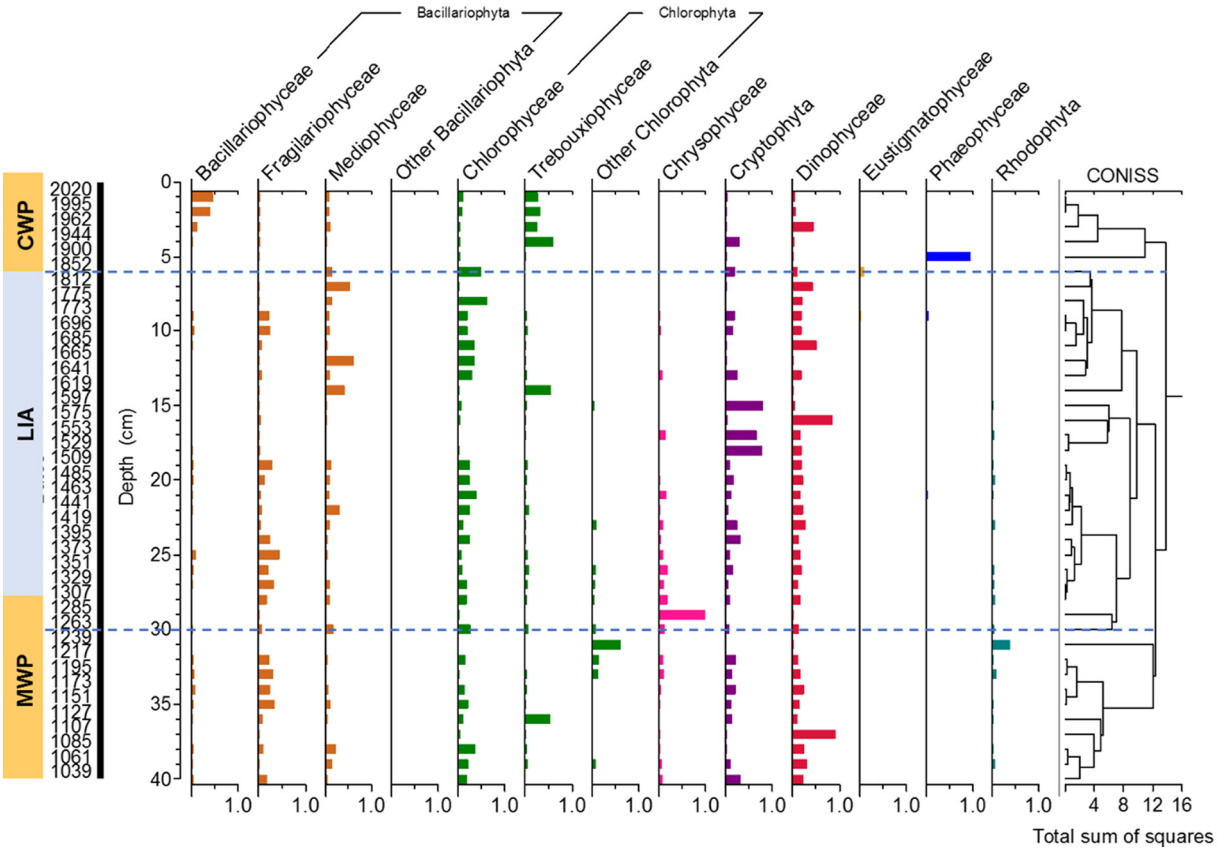

Fig. 3. Relative abundances of eukaryotic algae taxonomic groups across time in the Lake Yamzhog Yumco. The right panel shows results from constrained incremental sums of squares cluster analysis (CONISS) based on the relative abundances of eukaryotic algae groups among different layers. MWP, LIA, and CWP represent the Medieval Warm Period, Little Ice Age, and Current Warm period, respectively.

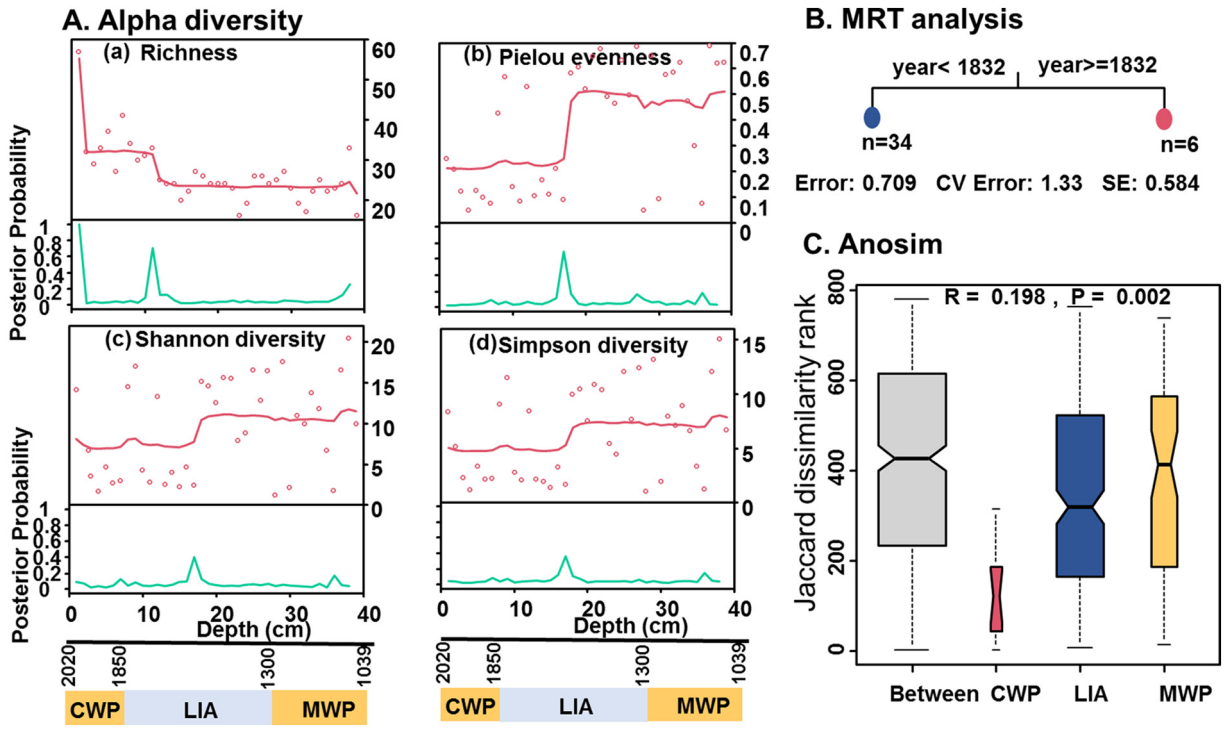

Fig. 4. Temporal trends in α diversity of eukaryotic algal communities based on Bayesian change point (*bcp*) test in the left panel (A), the breakpoints analyzed by multivariate regression tree (MRT) models based on OTU matrices (B), and violin plots showing the Jaccard dissimilarity of eukaryotic algal communities among the three historical phases estimated by analysis of similarities (ANOSIM) tests. The value of poster probability ≥0.5 that is considered as a significant change point. n is the number of samples in each group.

temperature and precipitation on eukaryotic algal communities, and demonstrate that both factors affected communities via nutrient dynamics (Wang et al., 2016).

4. Discussion

Pigment analysis of Lake Yamzhog Yumco sediment core profiles demonstrated that algal biomass significantly increased following ~1850 CE (Fig. 2), consistent with records for Tibetan Plateau lakes that indicate increased algal production after the 1800's (Lami et al., 2010; Hu et al., 2014). These consistent behaviors of increased autochthonous production in most Tibetan plateau lakes can be interpreted as responses to long-term climate change and land-use variation in recent decades (Lami et al., 2010; Jimenez et al., 2018; Liang et al., 2021). *sed*DNA analysis was used to reconstruct algal community succession in the Tibetan plateau lake studied here, revealing that eukaryotic algal community succession was almost nearly synchronous with climate change across the past millennium, with three successional periods corresponding to the MWP (approximately 1000–1250 CE), the LIA (1250–1850 CE), and the CWP (1850–2020 CE) (Fig. 3, Fig. 4). Likewise, vegetation types in the basin have alternated between alpine meadows and steppe patterns due to cold-moist/warm-dry climate oscillations over the past 2000 years (Guo et al., 2018). Therefore, climate-induced environmental changes in this region may influence aquatic and terrestrial ecosystems (Chen et al., 2013; Yang et al., 2014; Lin et al., 2017; Zhang et al., 2020).

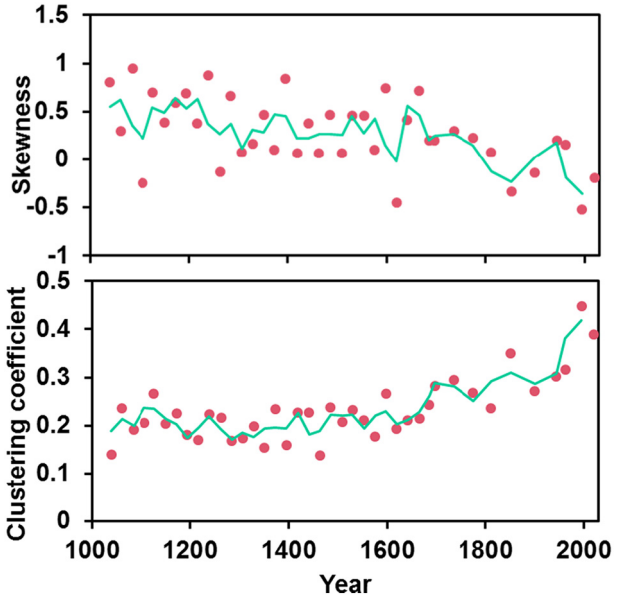

Fig. 5. Temporal variation in skewness and clustering coefficient for the frequency distribution of connected OTU pairings for eukaryotic algal communities in Lake Yamzhog Yumco. Traces show moving average regressions.

Climate warming can induce profound influences on eukaryotic algal communities either directly through higher temperatures or indirectly through variation in nutrient levels (Savichtcheva et al., 2015; Lin et al., 2017). Climate warming is associated with increased algal biomass by improving the rate of algal enzymatic reactions and assisting recruitment and growth mechanisms (O'Beirne et al., 2017; Righetti et al., 2019). Although Cyanobacteria were not the dominant photosynthetic group in this alpine lake due to the low temperatures, the dominant Bacillariophyta and Chlorophyta groups also significantly responded to temperature increases (Fig. 3; Woolway et al., 2020). In addition, warming-enhanced permafrost thawing and glacier retreat could be partly responsible for additional nutrient inputs into the lake from increased surface runoff (Zou et al., 2017), consistent with the observation that climate significantly impacted nutrient levels based on PLS-PM modeling (Fig. 6d). The lower altitude limit of permafrost in the southern Tibetan Plateau has moved up 50–80 m in the past 30 years, while the thickness of the active soil layer has increased by 0.15–0.5 m across the past decade, thereby influencing

soil moisture and soil water-holding capacity that in turn accelerates desertification processes (Yang et al., 2010; Zou et al., 2017). Moreover, Tibetan glaciers have exhibited dramatic recession in recent decades that could lead to increased glacial meltwaters that are rich in organic matter and nutrients that could alter the geochemistry of lacustrine ecosystems (Slemmons and Saros, 2012; Yao et al., 2012; Nie et al., 2017).

Precipitation also has a range of consequences on aquatic ecosystems by increasing nutrient loads at non-point sources and diluting chemical substances (e.g., salinity) by increasing lake water volumes (Chen et al., 2013; Tao et al., 2020). Annual precipitation has increased in Lake Yamzhog Yumco across recent decades, while evaporation has intensified with increased temperature, leading to decreasing lake water levels and areas (Zhang et al., 2011; Sun et al., 2021). The effects of precipitation on eukaryotic algal communities in this lake likely primarily occurs through the increase of runoff nutrients and dissolved organic matter availability in association with increased temperatures (Woolway et al., 2020). Wetter and warmer climates have been observed to lead to 'browner' lakes from terrestrial inputs of dissolved organic matter that would then alter the

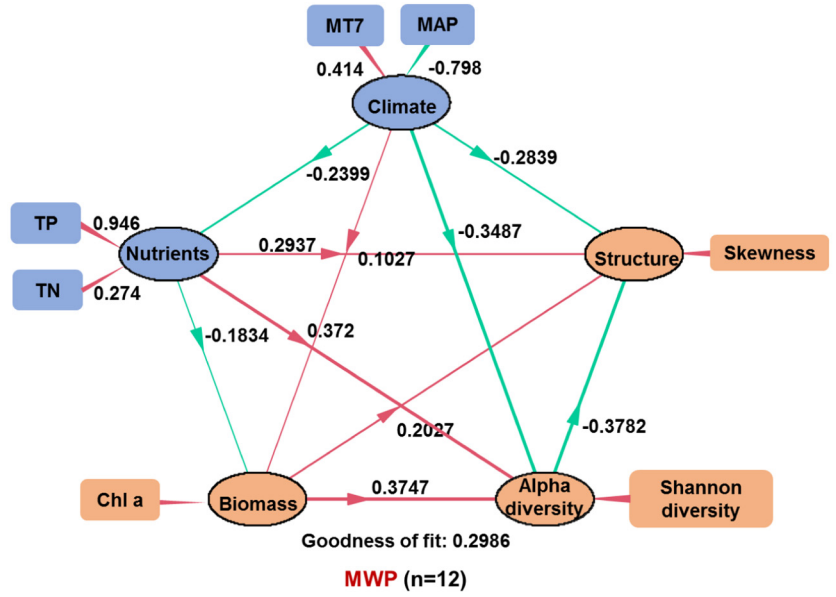

(a)

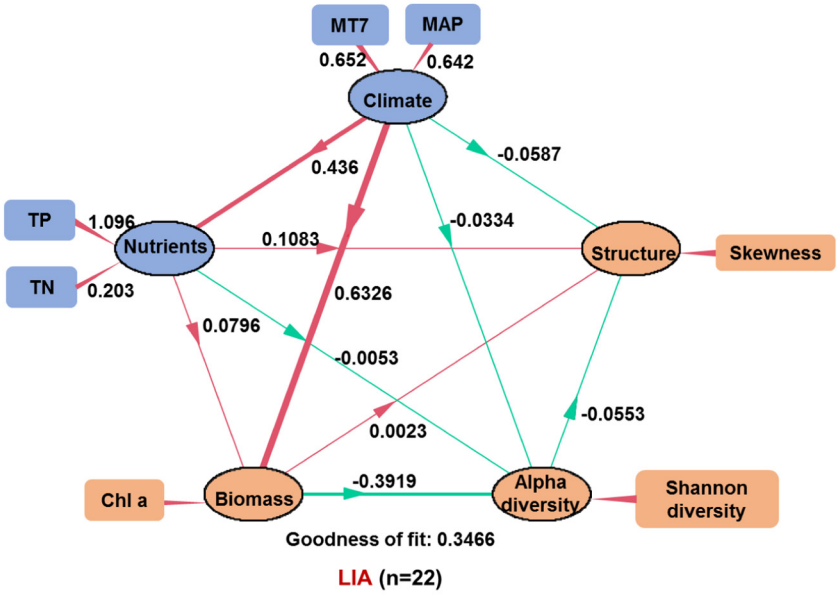

(b)

Fig. 6. The direct effects of climate variables and nutrients on the algal biomass, diversity and structure of eukaryotic algal community by the partial least squares path modeling (PLS-PM) during three historical phases, Medieval Warm Period (a), Little Ice Age (b), and Current Warm period (c), and the entire period (d). Variables in orange represent response variables and variables in blue the explanatory variables. The red and green lines represent positive and negative effects, respectively.

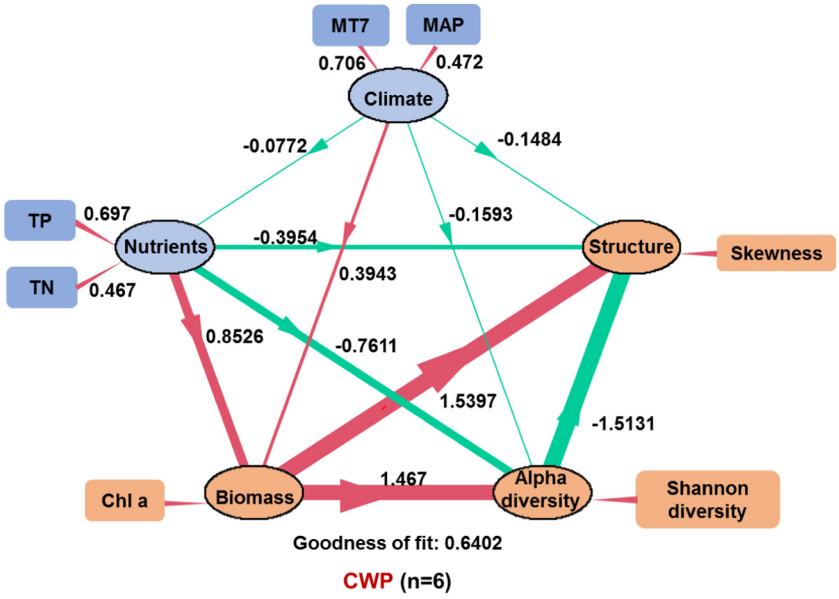

(c)

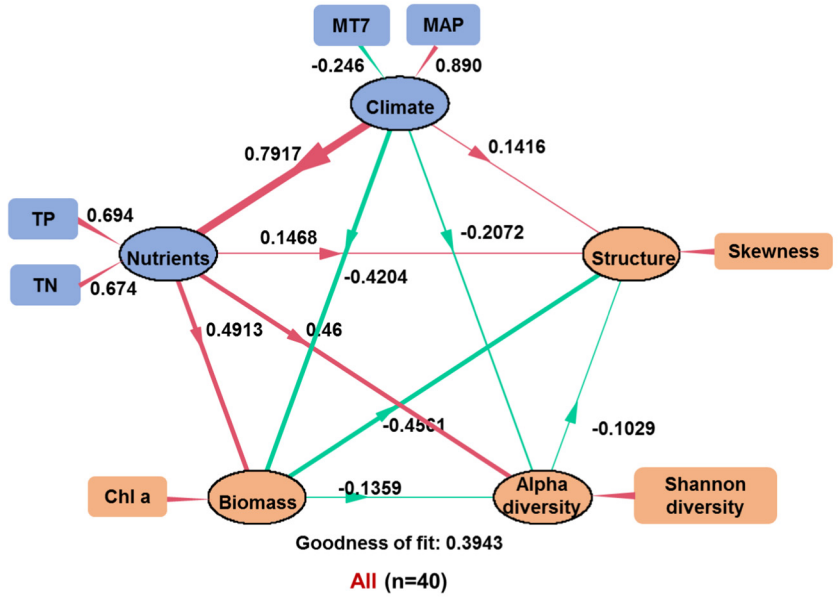

(d)

Fig. 6 (*continued*).

functioning of aquatic food webs, while affecting nutrient availability and water quality in addition to community composition and productivity (de Wit et al., 2016; Jimenez et al., 2018). Thus, the pressing need is to take measures, such as restoration of vegetation cover and buffer strips, to mitigate the effects of climate change on the water quality of alpine lake ecosystems that is associated with increases in phytoplankton biomass and shifts in community composition (Slemmons and Saros, 2012; Jimenez et al., 2018; Tao et al., 2020).

5. Conclusions

In this study, eukaryotic algal community temporal dynamics in a Tibetan Plateau lake were evaluated across the past 2000 years. Sedimentary pigment analysis indicated a significant increase in lacustrine primary productivity after ~1850 CE, while sedimentary DNA records indicated the succession of eukaryotic algal communities across the WMP, LIA, and CWP periods, consistent with established climatic periods. Paleolimnological evidence suggested that climate change contributed to primary production and eukaryotic algal community succession in the Tibetan Plateau lake. Warming can also lead to permafrost thawing and glacier retreat that can combine with increased precipitation, likely leading to increases in phytoplankton biomass and shifts in community composition due to increased terrestrial nutrient loading. These results suggest that effective restoration of vegetation cover may help mitigate the effects of warmer and wetter climates from modern climatic change on aquatic ecosystems in Tibetan Plateau alpine lakes.

CRediT authorship contribution statement

S. Huo, H. Zhang: Conceptualization, Methodology, Writing - original draft preparation. **J. Wang, J. Chen:** Collection- Analysis of data, Writing- original draft preparation. **F. Wu:** reviewing and editing.

Declaration of competing interest

The authors declare that they have no known competing financial interests or personal relationships that could have appeared to influence the work reported in this paper.

Acknowledgements

The National Natural Science Foundation of China (No. 51922010) and the National Key Research and Development Program of China (2017YFA0605003) supported this study. We thank LetPub (www.letpub.com) for linguistic assistance and pre-submission expert review.

Appendix A. Supplementary data

Supplementary data to this article can be found online at https://doi.org/10.1016/j.scitotenv.2022.154636.

References

Anderson, M.J., 2014. Permutational Multivariate Analysis of Variance (PERMANOVA). John Wiley & Sons, Ltd, Chichester https://doi.org/10.1002/9781118445112.stat07841.
Anderson-Carpenter, L.L., Mclachlan, J.S., Jackson, S.T., Kuch, M., Lumibao, C.Y., Poinar, H.N., 2011. Ancient DNA from lake sediments: bridging the gap between paleoecology and genetics. BMC Evol. Biol. 11 (1), 30.
Bennett, K.D., 1996. Determination of the number of zones in a biostratigraphical sequence. New Phytol. 132, 155–170.
Berry, D., Widder, S., 2014. Deciphering microbial interactions and detecting keystone species with co-occurrence networks. Front. Microbiol. 5 (219), 1–14.
Capo, E., Debroas, D., Arnaud, F., Perga, M.-E., Chardon, C., Domaizon, I., 2017. Tracking a century of changes in microbial eukaryotic diversity in lakes driven by nutrient enrichment and climate warming. Environ. Microbiol. 19 (7), 2873–2892.
Caporaso, J.G., Kuczynski, J., Stombaugh, J., Bittinger, K., Bushman, F.D., Costello, E.K., Fierer, N., Peña, A.G., Goodrich, J.K., Gordon, J.I., 2010. QIIME allows analysis of high-throughput community sequencing data. Nat. Methods 7, 335–336.
Carter, J.F., Fry, B., 2013. Ensuring the reliability of stable isotope ratio data—beyond the principle of identical treatment. Anal. Bioanal. Chem. 405, 2799–2814.
Chen, H., Zhu, Q., Peng, C., Wu, N., Wang, Y., Fang, X., et al., 2013. The impacts of climate change and human activities on biogeochemical cycles on the Qinghai-Tibetan plateau. Glob. Chang. Biol. 19 (10), 2940–2955.
De'ath, G., 2002. Multivariate regression trees: a new technique for modeling species environment relationships. Ecology 83, 1105–1117.
De'ath, G., 2014. MVPART: Multivariate Partitioning. R Package Version 1.6-2. https://CRAN.R-project.org/package=mvpart.
Domaizon, I., Winegardner, A., Capo, E., Gauthier, J., Gregory-Eaves, I., 2017. DNA-based methods in paleolimnology: new opportunities for investigating long-term dynamics of lacustrine biodiversity. J. Paleolimnol. 58 (1), 1–21.
Fritsch, F.N., Carlson, R.E., 1980. Monotone piecewise cubic interpolation. SIAM J. Numer. Anal. 17, 238–246.
Guo, C., Ma, Y., Meng, H., Hu, C., Li, D., Liu, J., et al., 2018. Changes in vegetation and environment in yamzhog yumco lake on the southern tibetan plateau over past 2000 years. Palaeogeogr. Palaeoclimatol. Palaeoecol. 501, 30–44.
Hair, J.F., Risher, J.J., Sarstedt, M., Ringle, C.M., 2019. When to use and how to report the results of PLS-SEM. Eur. Bus. Rev. 31 (1), 2–24.
Hu, Z., Anderson, N.J., Yang, X., McGowan, S., 2014. Catchment-mediated atmospheric nitrogen deposition drives ecological change in two alpine lakes in SE Tibet. Glob. Chang. Biol. 20 (5), 1614–1628.
Ibrahim, A., Capo, E., Wessels, M., Martin, I., Meyer, A., Schleheck, D., Epp, L., 2020. Anthropogenic impact on the historical phytoplankton community of Lake Constance reconstructed by multimarker analysis of sediment-core environmental DNA. Mol. Ecol. 00, 1–17.
Jiang, T., Yu, Z., Qi, Z., Chai, C., Qu, K., 2017. Effects of intensive mariculture on the sediment environment as revealed by phytoplankton pigments in a semi-enclosed bay, South China Sea. Aquac. Res. 48 (4), 1923–1935.
Jimenez, L., Ruhland, K.M., Jeziorski, A., Smol, J.P., Perez- Martinez, C., 2018. Climate change and Saharan dust drive recent cladoceran and primary production changes in remote alpine lakes of Sierra Nevada, Spain. Glob. Chang. Biol. 24, e139–e158.
Keck, F., Millet, L., Debroas, D., Etienne, D., Galop, D., Rius, D., Domaizon, I., 2020. Assessing the response of micro-eukaryotic diversity to the Great Acceleration using lake sedimentary DNA. Nat. Commun. 11 (1), 3831.
Lami, A., Turner, S., Musazzi, S., Gerli, S., Guilizzoni, Piero, Rose, N.L., et al., 2010. Sedimentary evidence for recent increases in production in Tibetan plateau lakes. Hydrobiologia 648, 175–187.
Lewis, S.L., Maslin, M.A., 2015. Defining the anthropocene. Nature 519 (7542), 171–180.
Li, D., Yao, P., Bianchi, T.S., Zhao, B., Pan, H., Zhang, T., Wang, J., Xu, B., Yu, Z., 2015. Historical reconstruction of organic carbon inputs to the East China Sea inner shelf: implications for anthropogenic activities and regional climate variability. The Holocene 25, 1869–1881.
Liang, J., Lupien, R.L., Xie, H., Vachula, R.S., Stevenson, M.A., Han, B., et al., 2021. Lake ecosystem on the Qinghai–Tibetan Plateau severely altered by climatic warming and human activity. Palaeogeogr. Palaeoclimatol. Palaeoecol. 576, 110509.
Lin, Q., Xu, L., Hou, J., Liu, Z., Jeppesen, E., Han, B.P., 2017. Responses of trophic structure and zooplankton community to salinity and temperature in Tibetan lakes: implication for the effect of climate warming. Water Res. 124 (1), 618.
Magoč, T., Salzberg, S.L., 2011. FLASH: fast length adjustment of short reads to improve genome assemblies. Bioinformatics 27 (21), 2957–2963. http://ccb.jhu.edu/software/FLASH/.
Monchamp, M.E., Spaak, P., Domaizon, I., Dubois, N., Bouffard, D., Pomati, F., 2018. Homogenization of lake cyanobacterial communities over a century of climate change and eutrophication. Nat. Ecol. Evol. 2 (2), 317–324.
Murphy, J., Riley, J.P., 1962. A modified single solution method for the determination of phosphate in natural waters. Anal. Chim. Acta 27, 31–36.
Newman, M., 2006. Modularity and community structure in networks. Proc. Natl. Acad. Sci. U. S. A. 103 (23), 8577–8582.
Nie, Y., Sheng, Y., Liu, Q., Liu, L., Liu, S., Zhang, Y., Song, C., 2017. A regional-scale assessment of Himalayan glacial lake changes using satellite observations from 1990 to 2015. Remote Sens. Environ. 189, 1–13.
O'Beirne, M.D., Werne, J.P., Hecky, R.E., Johnson, T.C., Katsev, S., Reavie, E.D., 2017. Anthropogenic climate change has altered primary productivity in Lake Superior. Nat. Commun. 8 (1), 1–8.
Oksanen, J., Blanchet, F.G., Friendly, M., Kindt, R., Legendre, P., McGlinn, D., et al., 2020. vegan: Community Ecology Package. R Package Version: 2.5−7. https://cran.r-project.org/web/packages/vegan/index.html.
Pepin, N., Bradley, R.S., Diaz, H.F., Baraer, M., Caceres, E.B., Forsythe, N., et al., 2015. Elevation-dependent warming in mountain regions of the world. Nat. Clim. Chang. 5, 424–430.
Posch, T., Köster, O., Salcher, M.M., Pernthaler, J., 2012. Harmful filamentous cyanobacteria favoured by reduced water turnover with lake warming. Nat. Clim. Chang. 2 (11), 809–813.
Pruesse, E., Quast, C., Knittel, K., Fuchs, B.M., Ludwig, W.G., Peplies, J., Glöckner, F.O., 2007. SILVA: a comprehensive online resource for quality checked and aligned ribosomal RNA sequence data compatible with ARB. Nucleic Acids Res. 35, 7188–7196. https://www.arb-silva.de/contact/.
Qiao, B., Zhu, L., Yang, R., 2019. Temporal-spatial differences in lake water storage changes and their links to climate change throughout the Tibetan plateau. Remote Sens. Environ. 222, 232–243.
Ramette, A., 2007. Multivariate analyses in microbial ecology. FEMS Microbiol. Ecol. 62, 142–160.
Reimer, P.J., Bard, E., Bayliss, A., 2013. Intcal13 and marine13 radiocarbon age calibration curves 0~50,000 years cal BP. Radiocarbon 55 (4), 1869–1887.
Righetti, D., Vogt, M., Gruber, N., Psomas, A., Zimmermann, N.E., 2019. Global pattern of phytoplankton diversity driven by temperature and environmental variability. Sci. Adv. 5 (5), eaau6253.
Roy, S., Llewellyn, C.A., Egeland, E.S., Johnsen, G.J., 2011. Phytoplankton Pigments. Cambridge University Press, Cambridge (ISBN: 9781107000667).
Royden, L.H., Burchfiel, B.C., Hilst, R., 2008. The geological evolution of the Tibetan Plateau. Science 321, 1054–1058.
Savichtcheva, O., Debroas, D., Perga, M.E., Arnaud, F., Villar, C., Lyautey, E., Kirkham, A., Chardon, C., Alric, B., Domaizon, I., 2015. Effects of nutrients and warming on Planktothrix dynamics and diversity: a palaeolimnological view based on sedimentary DNA and RNA. Freshw. Biol. 60 (1), 31–49.
Schloss, P.D., Westcott, S.L., Ryabin, T., Hall, J.R., Hartmann, M., Hollister, E.B., 2009. Introducing mothur: open-source, platform-independent, community-supported software for describing and comparing microbial communities. Appl. Environ. Microbiol. 75 (23), 7531–7541.
Slemmons, K., Saros, J.E., 2012. Implications of nitrogen-rich glacial meltwater for phytoplankton diversity and productivity in alpine lakes. Limnol. Oceanogr. 57 (6), 1651–1663.
Solorzano, L., Sharp, J.H., 1980. Determination of total dissolved nitrogen in natural waters. Limnol. Oceanogr. 25, 751–754.
Strom, S., 2008. Microbial ecology of ocean biogeochemistry: a community perspective. Science 320 (5879), 1043–1045.
Sun, R., Zhang, X., Fraedrich, K., You, Q., 2021. CMIP5 climate projections for the Yamzhog Yumco basin: an environmental testbed for alpine lakes. Theor. Appl. Climatol. 143, 795–808.
Tao, S., Fang, J., Ma, S., Cai, Q., Xiong, X., Tian, D., et al., 2020. Changes in china's lakes: climate and human impacts. Natl. Sci. Rev. 7, 132–140.
Tse, T.J., Doig, L.E., Tang, S., Zhang, X.H., Sun, W.M., Wiseman, S.B., Feng, C.X., Liu, H.L., Giesy, J.P., Hecker, M., Jones, P.D., 2018. Combining high-throughput sequencing of sedaDNA and traditional palaeolimnological techniques to infer historical trends in cyanobacterial communities. Environ. Sci. Technol. 52 (12), 6842–6852.
Wang, J., Pan, F., Soininen, J., Heino, J., Shen, J., 2016. Nutrient enrichment modifies temperature-biodiversity relationships in large-scale field experiments. Nat. Commun. 7, 13960.
Wang, X., Erdman, C., Emerson, J.W., 2018. bcp: Bayesian Analysis of Change Point Problems. R Package Version 4.0.3. https://cran.r-project.org/web/packages/bcp/index.html.

Wang, R., Dearing, J., Doncaster, C., Yang, X., Shen, J., 2019. Network parameters quantify loss of assemblage structure in human-impacted lake ecosystems. Glob. Chang. Biol. 25 (11), 3871–3882.

de Wit, H.A., Valinia, S., Weyhenmeyer, G.A., Futter, M.N., Kortelainen, P., Austnes, K., et al., 2016. Current browning of surface waters will be further promoted by wetter climate. Environ. Sci. Technol. Lett. 3 (12), 430–435.

Woolway, R.I., Kraemer, B.M., Lenters, J.D., Merchant, C.J., O'Reilly, C.M., Sharma, S., 2020. Global lake responses to climate change. Natur. Rev. Earth Environ. https://doi.org/10.1038/s43017-020-0067-5.

Wu, G., Duan, A., Liu, Y., Mao, J., Ren, R., Bao, Q., et al., 2015. Tibetan Plateau climate dynamics: recent research progress and outlook. Natl. Sci. Rev. 2, 100–116.

Yang, M., Nelson, F.E., Shiklomanov, N.I., Guo, D., Wan, G., 2010. Permafrost degradation and its environmental effects on the Tibetan Plateau: a review of recent research. Earth Sci. Rev. 103, 31–44.

Yang, H., Wu, J., Qin, J., Lin, C., Tang, W., Chen, Y., 2014. Recent climate changes over the Tibetan plateau and their impacts on energy and water cycle: a review. Glob. Planet. Chang. 112, 79–91.

Yao, T., Thompson, L., Yang, W., Yu, W., Gao, Y., Guo, X., et al., 2012. Different glacier status with atmospheric circulations in Tibetan Plateau and surroundings. Nat. Clim. Chang. 2, 663–667.

Zhang, G., Xie, H., Kang, S., Yi, D., Ackley, S.F., et al., 2011. Monitoring lake level changes on the Tibetan plateau using Icesat altimetry data (2003–2009). Remote Sens. Environ. 115, 1733–1742.

Zhang, G., Yao, T., Shum, C.K., Yi, S., Yang, K., Xie, H., et al., 2017. Lake volume and groundwater storage variations in Tibetan Plateau's endorheic basin. Geophys. Res. Lett. 44, 5550–5560.

Zhang, H., Huo, S., Yeager, K.M., He, Z., Xi, B., Li, X., et al., 2019. Phytoplankton response to climate changes and anthropogenic activities recorded by sedimentary pigments in a shallow eutrophied lake. Sci. Total Environ. 647, 1398–1409.

Zhang, G., Yao, T., Xie, H., Yang, K., Zhu, L., Shum, C.K., et al., 2020. Response of Tibetan Plateau lakes to climate change: trends, patterns, and mechanisms. Earth Sci. Rev. 208, 103269.

Zhang, H., Huo, S., Wang, R., Xiao, Z., Li, X., Wu, F., 2021a. Hydrologic and nutrient-driven regime shifts of cyanobacterial and eukaryotic algal communities in a large shallow lake: evidence from empirical state indicator and ecological network analyses. Sci. Total Environ. 783, 147059.

Zhang, H., Huo, S., Xiao, Z., He, Z., Yang, J., Yeager, K.M., Li, X., Wu, F., 2021b. Climate and nutrient-driven regime shifts of cyanobacterial communities in low-latitude plateau lakes. Environ. Sci. Technol. 55 (5), 3408–3418.

Zhe, M., Zhang, X., 2021. Time-lag effects of NDVI responses to climate change in the Yamzhog Yumco basin, south tibet - sciencedirect. Ecol. Indic. 124, 107431.

Zhe, M., Zhang, X., Wang, B., Sun, R., Zheng, D., 2017. Hydrochemical regime and its mechanism in Yamzhog Yumco Basin, South Tibet. J. Geogr. Sci. 27 (9), 1111–1122.

Zou, D., Zhao, L., Sheng, Y., Chen, J., Hu, G., Wu, T., et al., 2017. A new map of permafrost distribution on the Tibetan Plateau. Cryosphere 11, 2527–2542.